Anomaly Detection and Localization in NFV Systems by Utilizing Masked-Autoencoder and XAI

Seyed Soheil Johari*, Nashid Shahriar†, Massimo Tornatore‡, Raouf Boutaba*, Aladdin Saleh§ *David R. Cheriton School of Computer Science, University of Waterloo, {ssjohari | rboutaba}@uwaterloo.ca
†Department of Computer Science, University of Regina, nashid.shahriar@uregina.ca
‡Politecnico di Milano, massimo.tornatore@polimi.it
§Rogers Communications Canada Inc., aladdin.saleh@rci.rogers.com

***Abstract*—The increasing integration of Network Functions Virtualization (NFV) systems within mobile edge computing and core networks has accentuated the need for robust anomaly detection and localization methodologies. This heightened necessity is primarily driven by the increased complexity inherent in NFV architectures, which require sophisticated mechanisms to ensure the resilience, security, and performance of mobile networks. Conventional supervised learning approaches are hindered by the scarcity of labeled data for faulty scenarios. Consequently, Unsupervised Learning (UL) methods have garnered significant attention for their potential to detect anomalies without the need for labeled data. However, UL methods are susceptible to even minor levels of anomalous samples in the training data, termed as contamination, which can severely compromise their performance. In this paper, we propose a novel approach for anomaly detection in NFV systems based on the Noisy-Student technique. Our approach addresses the challenge of training-data contamination by employing a density-estimation teacher model to pseudo-label the training data, coupled with a weakly-supervised student model based on a Masked Autoencoder that is trained on the obtained pseudo-labeled samples. This framework not only enhances robustness against contamination but also leverages the contamination to improve anomaly-detection accuracy. Furthermore, we tackle the problem of anomaly localization in NFV systems, which remains challenging due to the absence of labeled data. For anomaly localization, we introduce a heuristic tailored for our anomaly detection model and two Explainable Artificial Intelligence (XAI)-based approaches applicable to any detection model. Extensive experiments conducted on three diverse NFV datasets demonstrate the superiority of our proposed solutions. Our methods outperform existing techniques by up to 24% in anomaly detection and up to 22% in anomaly localization, as measured by F1-score. These findings underscore the efficacy of our approach in enhancing the reliability and performance of anomaly detection and localization in NFV systems within mobile computing environments.**

I. Introduction

Virtualization represents a revolutionary change in the networking industry, similar to the change brought in the computer industry in the 80's. A promising application of virtualization in networking is NFV. NFV allows decoupling network or service functions from the underlying hardware by implementing them as software appliances, called Virtual Network Functions (VNFs), on virtualized commodity hardware. Furthermore, with the continuous advancement and widespread adoption of VNFs especially in mobile computing environments, the potential for achieving near-hardware performance and realizing substantial opportunities for network optimization and cost reduction has become increasingly evident. As NFV deployments continue to proliferate in mobile computing, the effective implementation of anomaly detection and localization techniques is crucial to ensure the resilience, security, and efficiency of these dynamic and complex systems, ultimately enabling the realization of their full potential in enhancing mobile network capabilities [1, 2]. Nonetheless, provisioning and managing VNF-based services introduce additional complexity due to dynamic network topologies, multiple layering, and lack of network visibility. This increased complexity makes VNFs more failure-prone than dedicated hardware-based solutions [3], [4], [5]. Therefore, detecting anomalous behavior in an NFV system and localizing its root cause is of paramount importance to ensure high reliability for virtualized services.

The complex inter-dependencies and multi-faceted fault characteristics in NFV systems render traditional anomaly-detection and localization approaches inefficient as they typically identify malfunctions by metrics crossing a threshold configured by some field expert [6], [7]. On the other hand, Machine Learning (ML) methods, in particular Deep Learning (DL) methods, have shown promising results in developing adaptive and efficient mechanisms to detect and localize potential anomalies in a dynamic NFV system by capturing hidden dependencies among a variety of performance metrics [8], [9]. However, most of these existing ML-based approaches utilize Supervised Learning (SL) algorithms that require abundant labeled faulty instances to achieve satisfactory performance. Unfortunately, labeled network faulty data is a scarce resource and generally unavailable in sufficient volumes for two main reasons: *i)* labeling data often requires domain experts to annotate logs of anomalous scenarios, and *ii)* only a small amount of the monitored data from the NFV system is related to faulty scenarios [7].

UL-based anomaly detection on multi-dimensional data can help alleviate the need for abundant labeled faulty instances. In addition to reducing the reliance on labeled data and domain experts' knowledge, another benefit of a UL approach from an operational point of view is that it would not be biased on some specific failure scenarios and can provide a more generalized protection against many sorts of anomalous behaviors in the NFV system. For example, UL methods based on Recurrent Neural Networks (RNNs) are well-known for anomaly detection on temporal data, however, training RNNs generally is a long and computationally expensive process that requires a large volume of training data [10]. Therefore, RNNs are not suitable for NFV environments with dynamic topologies where periodic software updates often change the system functionality, with the consequence that the ML models need to be often re-tuned with newly collected data [10].

Autoencoder is another popular UL method that generally trains faster and requires much less training data than RNNs to reach a satisfactory performance [10]. Autoencoders have been utilized for unsupervised anomaly detection in many network management tasks, including anomaly detection in NFV architectures [6], [11]. These methods assume the availability of a training dataset that purely consists of normal instances. However, it is often unavoidable that the historical data collected from the NFV system includes a few anomalous samples, i.e., we expect historical data to have some degree of contamination. Different studies have shown that even small percentages of contamination in the training data can significantly degrade the performance of Autoencoders in UL anomaly-detection methods [12], [13].

In this paper, we propose a novel unsupervised anomaly-detection approach for NFV systems when training data is contaminated (a problem arising in most practical scenarios). Inspired by the Noisy-Student [14] concept used in computer vision, we first train a Deep Autoencoding Gaussian Mixture Model (DAGMM) [13], (i.e., a UL anomaly-detection method based on density estimation) on the contaminated training data as the teacher model. Then, we use DAGMM to remove potential anomaly instances (i.e., to clean the training data), and from these removed instances, we pseudo-label a few samples that DAGMM has classified as anomalies with very high confidence (pseudo-labeling [15] is the process of using a trained ML model to predict labels for unlabelled data). In this way, we compensate for some of the information that we potentially lose during the data cleaning process. The cleaned dataset and pseudo-labeled anomalies are then fed to the student model, which is our novel architecture consisting of a Masked Autoencoder (MAE) [16] cascaded with a weakly-supervised anomaly-detection model called Deviation Network [16]. We also use data augmentation in feature space [17], a data augmentation method proposed for non-image data, to add noise to the extracted pseudo-labeled anomalies to improve the model's generalization.

Once anomaly detection is successfully done with the approach described above, we focus on developing an unsupervised approach for anomaly localization, i.e., localizing the anomalous VNF after an anomaly is detected. Localization is also a challenging task in a UL approach, as there might be no labeled anomalous instances in the training data, and distinguishing between different anomaly locations can only be done by comparing the detected anomaly with normal instances. In this paper, we first propose a heuristic method that utilizes the output of our MAE-based detection model for different masking scenarios of the MAE to determine the anomaly location. While the proposed heuristic is specifically designed for the MAE-based detection model, we also propose two general localization methods based on XAI that are applicable to any black-box anomaly detection model. We show the effectiveness of our proposed solutions through comprehensive experimental evaluations on three datasets from different NFV testbeds. The first dataset is generated in an NFV-based test environment that simulates a 5G IP core network. The second dataset is from our experimental NFV testbed that resembles Multi-access Edge Computing (MEC) in topology. The last dataset is collected by [18] from the ClearWater project, which is an NFV-based open source implementation of an IP Multimedia Subsystem (IMS) for cloud platforms. In the evaluation results, we observed improvement up to 24% in anomaly detection and up to 22% in anomaly localization in terms of F1-score compared to the state-of-the-art methods.

This paper is an extended version of the work presented in [19]. In this extended version, we modified the student model of the anomaly detection architecture to learn more generalizable features from the input data through a MAE, which is a transformer-based Autoencoder model. As we will see in the next sections, utilizing MAE in the student model not only improves the anomaly detection performance, but can also provide valuable information for the localization task based on its output for different masking scenarios. Moreover, in the extended version, we compare our student model with other weakly-supervised methods from the state-of-the-art in a new set of experiments. We also compare our proposed anomaly detection method with SL methods in terms of generalization capability, and show that unlike SL models, our method is able to detect failure scenarios that are unseen during training. Finally, we expand our discussion of the related work and experimental results.

The rest of the paper is organized as follows. Section II discusses the related work. Section III is a detailed description of our problem formulation. Our anomaly-detection and localization approaches are detailed in Sections IV and V, respectively. Section VI presents experimental analysis using datasets from three distinct NFV testbeds, and finally, Section VII concludes the paper.

II. Related Work

A. ML-based Fault Detection and Diagnosis

Many works leveraged SL for fault detection and diagnosis, including fault management of NFV environments [7, 20–24]. Authors in [20] utilized text convolutional neural network (textCNN) and the BERT model [25] for classification of service chain failures based on logs containing key performance indicators (KPIs) of network components that can originate service quality degradation. The work in [21] used Random Forest (RF) as a supervised learning approach for detection and root cause localization of Virtual Machine anomalies in NFV infrastructures including anomalous CPU consumption, memory leaks, excessive number of disk accesses, packet losses, latency increases, and heavy workload. The authors in [22] trained Stacked and Bidirectional LSTM models on a large amount of multivariate time series data collected from the NFV system in cloud environments for early detection of performance degradation and service failures. Similar to [22], the proposed approach in [23] leveraged sequential deep learning methods like RNNs and Transformers to capture temporal dependencies and sequential patterns in the data for anomaly detection in VNF chains. Authors in [7] generated faulty scenarios of network latency, CPU resource shortage, and excessive disk I/O in the ClearWater IMS test-bed through fault injection tools, and evaluated the performance of RF, extreme gradient boosting (XGBOOST), max-likelihood classification, and K-nearest neighbors (KNN) methods in detecting and classifying the mentioned network failures.

However, as discussed earlier, SL methods require abundant labeled network-fault data that usually is unavailable in sufficient volumes. Some existing works addressed the issue of lack of labeled data by investigating unsupervised ML techniques [6, 11, 21, 26–30]. For example, Authors in [21] evaluated the performance of three shallow unsupervised anomaly detection approaches (Isolation Forest, Local Outlier Factor, and One-Class SVM) on a dataset collected from the Vodafone NFV infrastructure that spans across multiple data centers in 11 European countries. A common Deep UL approach that is shown to outperform shallow UL methods for high-dimensional data consists in training an Autoencoder on a dataset consisting of only normal samples and performing anomaly detection based on the overall reconstruction error of the Autoencoder. This type of Autoencoder-based UL method has been used in [6] and [26] for anomaly detection in an NFV architecture, in [11] for anomaly detection in Radio Access Network (RAN) cell trace data collected from multiple Evolved NodeBs, in [27] for detecting anomalous symptoms in 5G RAN, and in [28] for anomaly detection on a cloudified mobile core architecture. However, all these works assume the availability of a training dataset that consists only of normal samples *with no contamination*.

B. Unsupervised Anomaly Detection with Contamination

Some existing studies from the ML field (e.g., [12], [13]) addressed the issue of training-data contamination for unsupervised anomaly detection on multi-variate data. Authors in [12] and [13] increase robustness against contamination by performing density estimation on the features extracted by the Autoencoder prior to anomaly detection. However, contamination still causes a significant degradation in the performance of these methods (partial robustness), while our approach even leverages the contamination to improve anomaly-detection performance ([13] is one of our compared approaches).

C. Weakly-supervised Anomaly Detection

Some works utilize weakly-supervised methods to leverage a limited number of labeled anomalous samples for boosting the anomaly detection performance. For instance, the approach in [31] uses a pair of VAE models, one model trained on the unlabeled data for learning reconstruction of normal samples, and another model which initially is an exact copy of the first trained VAE model, but fine-tuned on the limited number of labeled anomalous samples. At the end, the difference between the anomaly scores calculated by the two VAE models is considered as the ultimate metric for anomaly detection. In the experimental evaluations on eBay's search back-end systems, it is shown that this method outperforms the supervised ensemble method designed by domain experts at eBay. Similarly, the authors of [32] apply the cluster centers algorithm as a weakly-supervised method for anomaly detection on a real-world dataset from a facility monitoring system. They train k-means algorithm on unlabeled data to learn normal operational modes (the centers of k-means). Afterwards, they calculate an anomaly score for each test sample based on the distance of that sample from the nearest center and also on its distance from the closest labeled anomaly sample. Moreover, there are many weakly-supervised methods proposed in the ML literature for anomaly detection of multi-dimensional data, including DevNet [16], V-DevNet [33], D-SAD [34], and PRO [35]. We describe these approaches with more detail in Section VI.D, as they are implemented and evaluated in our experimental analysis.

D. Anomaly Localization

Different types of anomaly-localization techniques were proposed for fault diagnosis in network management. Model-based localization methods leverage the knowledge of network topology to build abstraction models, such as dependency graphs, to represent correlations among different metrics and events of the network that can be used for fault localization [36–40]. However, these techniques are not suitable for NFV architectures that have dynamic topologies [7]. Some data-driven methodologies employ a labeled dataset to tackle root cause analysis through a multi-classification approach [41–44]. For instance, authors in [41] address root cause analysis for wireless network failures by treating it as a time-series classification task. They achieve this by converting time-series data into fixed-size feature vectors and then employing an ensemble method that combines XGBoost, rule set learning, attribution models, and graph algorithms. However, these methods require abundant labeled anomalous samples to achieve satisfactory performance.

When anomaly detection is performed by an Autoencoder, most existing unsupervised localization approaches try to localize the anomalous VNF by analyzing reconstruction errors of different features in the Autoencoder [45], [46]. However, it is shown that these approaches usually lead to poor localization performances [45]. More recently, XAI methods have been utilized for anomaly localization [11], [47]; however, the methods in these works only provide some basic information to facilitate the procedure for the domain experts. In contrast, in our paper, we use XAI algorithms to perform the anomaly-localization task in a fully automated manner.

III. Problem Formulation

We are monitoring the health state of an NFV system that consists of a network of k VNFs: $vnf^1, vnf^2, ..., vnf^k$. In each time step t, we collect n_j metrics from vnf^j and denote these metrics as $vnf_t^j \in \mathbb{R}^{1\times n_j}$. Examples of these metrics could be the general performance metrics shared by all the VNFs, such as CPU utilization and incoming/outgoing packet rates, or more exclusive performance metrics related to the functionality of each individual VNF that can vary from one VNF to another (e.g., call success ratio). Therefore, x_t, our data sample for time step t that represents the status of the entire NFV system consists of the combination of all the collected metrics from all the VNFs: $x_t = \{vnf_t^1, vnf_t^2, ..., vnf_t^k\} \in \mathbb{R}^{1\times d}$, where $d = \sum_{j=1}^{k} n_j$ is the total number of metrics collected from the NFV system.

We have the historical data of the first n time steps: $X = \{x_1, x_2, ..., x_n\}$, $X \in \mathbb{R}^{n \times d}$. We assume the system works in normal circumstances for most of this period; however, the historical data also includes some anomalous samples and is not entirely made of normal instances. Similar to [13], we assume up to 5% of the training data might consist of anomalous samples (i.e., up to 5% contamination in the training data). Given this historical data of the NFV system for the first n time steps as the training data, we have two objectives in this problem:

- Anomaly Detection: Detecting anomalous behavior of the system after time step n, i.e., determining the behavior of the system $y_{n+i} \in \{0, 1\}$ (0: normal, 1: anomaly), for samples $x^{test}_{n+i} \in \mathbb{R}^{1 \times d}$, $i > 0$.
- Anomaly Localization: Localizing the VNF responsible for the anomalous behavior of the system after the detection of an anomaly, i.e., determining r such that vnf^r is the location of the anomaly.

IV. Masked Noisy-Student-based Unsupervised Anomaly-Detection (MNSUAD) Approach

To overcome the issue of contamination in the training data, we propose an unsupervised anomaly-detection approach based on the Noisy-Student method and call it MNSUAD. The Noisy-Student method was introduced in [14] for leveraging unlabeled datasets in computer vision classification problems. In this method, a neural network is trained on the available labeled dataset to reach an initial good performance. Then, this neural network is used as the teacher model to generate pseudo-labels on the unlabeled dataset. Afterwards, another neural network (usually larger in size and with more parameters) is trained on the combination of labeled and pseudo-labeled data, and is called the student model. The key idea behind this method, which enables the student model to outperform the teacher model, lies in injecting noise into the input data via data augmentation during the student model's learning process. This augmentation enhances the student's ability to generalize, resulting in improved performance.

A. Teacher Model

In a Noisy-Student approach, we need a teacher model that achieves an initial good performance in the anomaly-detection task, and its predictions are utilized for training a student model that outperforms the teacher. In our problem, we do not have a labeled dataset to train the teacher with; instead, for the teacher model to achieve an initial good performance in anomaly detection, we train a Deep Autoencoding Gaussian Mixture Model (DAGMM) [13], an unsupervised anomaly-detection method, on a fraction (e.g., 40% in our experiments) of the training data, initially treating the training data as it has no contamination. We train the DAGMM on a fraction of the training data instead of the whole training data to avoid overfitting on the anomalous samples. In other words, DAGMM treats its training samples as normal instances, therefore, training it on a fraction of data (instead of all data) would lead to fewer false negatives when we are observing the teacher's prediction on the training data. Since we are interested in extracting pseudo-labeled anomalies from the training samples, having fewer false negatives is more desirable to us than having fewer false positives at this stage.

As we mentioned earlier, DAGMM is shown to be robust against contamination in the training data to some extent [13]; therefore, it is a good choice for our teacher model. The output of DAGMM for a sample is an energy value representing the sample's potential to be an anomaly. The higher the energy of a sample, the higher is the probability that the sample is an anomaly. After training DAGMM on a fraction of training data, we observe its prediction (energy) of the whole training samples and denote it as E_X:

$$E_X = DAGMM(X),\ E_X \in \mathbb{R}^{n \times 1} \tag{1}$$

B. Cleaning Training Data and Extracting Pseudo-labeled Anomalies

We consider $\rho_1\%$ of training samples with the lowest energy as a cleaned training dataset (X_c) that is expected to be much less contaminated than the original training data (thr_1 is defined as the ρ_1-th percentile of the energy values in E_X):

$$thr_1 = percentile^{\rho_1}(E_X) \tag{2}$$

$$X_c = X[E_X < thr_1],\ X_c \in \mathbb{R}^{s \times d} \tag{3}$$

In our experiments, we chose $\rho_1 = 93\%$ to disregard a slightly larger percentage than the highest considered contamination percentage (5%) in the training data. However, X_c still could be contaminated (to a lesser degree, though), and we potentially would lose some valuable information by disregarding $(100 - \rho_1)\%$ of the training data. To compensate for this lost information, we extract some pseudo-labeled anomalies from the training samples that have the highest energy calculated by the DAGMM method. If μ_E and σ_E are the average and standard deviation of the energy values of samples in X_c, then we define thr_2 as:

$$thr_2 = \mu_E + b \times \sigma_E, b \geq 1 \tag{4}$$

In our experimental analysis, we chose $b = 2$, but its value does not have a big impact on the performance of the approach as long as it is not too large. By this definition, most of the samples in X_c would have a lower energy value than thr_2, and a considerable number of anomalous samples in the training data would have a higher energy value than thr_2; therefore, we also separate all the training samples with higher energy values than thr_2 as the potential contamination data, and denote it as X_{cont}:

$$X_{cont} = X[E_X > thr_2] \tag{5}$$

Now, we define thr_3 to choose the top $\rho_2\%$ samples with the highest energy values (e.g., top 20%) in X_{cont} as pseudo-labeled anomalies, and denote as X_{anom} (training samples that DAGMM has classified as anomalies with very high confidence):

$$E_{cont} = DAGMM(X_{cont}) \tag{6}$$

$$thr_3 = percentile^{(100-\rho_2)}(E_{cont}) \tag{7}$$

$$X_{anom} = X_{cont}[E_{cont} > thr_3] \tag{8}$$

In a Noisy-Student method, the key idea for achieving a better performing student model is to add noise to the pseudo-labeled data through data augmentation to improve the generalization of the student model. Therefore, we utilize the data augmentation method for non-image data proposed in [17], called "data augmentation in feature space (DAiFS)," to add noise to the extracted pseudo-labeled anomalies. We denote the obtained noisy anomalous pseudo-label samples as $\tilde{X}_{anom}$:

$$\tilde{X}_{anom} = DAiFS(X_{anom}) \tag{9}$$

Then, our new training data that the student model of MN-SUAD will be trained on is the combination of X_c and $\tilde{X}_{anom}$:

$$X_{new} = \{X_c, \tilde{X}_{anom}\},\ X_{new} \in \mathbb{R}^{e \times d} \tag{10}$$

C. Student Model

The actual task of anomaly detection is performed by a weakly-supervised student model trained on $X_{new} = \{X_c, \tilde{X}_{anom}\}$, which treats the samples belonging to X_c as normal samples and samples in $\tilde{X}_{anom}$ as known anomalies. For the student model, we propose a novel architecture, consisting of an MAE [16] and a Deviation Network (DevNet), to be trained on X_{new}. The proposed student model is presented in Fig. 1. DevNet [16] is a weakly-supervised learning anomaly-detection approach that is designed to utilize a few available labeled anomalies to improve the anomaly-detection performance; therefore, it is a well-suited approach to take advantage of the extracted pseudo-labeled anomalies in our problem. In DevNet, a single anomaly score value is directly learned from the input sample by a neural network, and this anomaly score is the anomaly-detection criterion. However, since this anomaly score is a direct mapping from the input space to a single scalar value, DevNet might not perform well when dealing with high-dimensional data. Moreover, DevNet typically requires a large number of training samples to avoid overfitting, which might not be available in our case. To address both of these issues, for the student model, we integrate DevNet with an MAE in a novel architecture, where Devnet learns its anomaly score from the rich features learned by the MAE from the input data, instead of learning it directly from the input samples. MAE is a transformer-based Auto-encoder model that has been shown to learn very generalizable representation from raw data [16]. These generalizable features contain valuable information regarding the anomalous behavior of the input samples, thus, can improve the performance of DevNet and also the scalability of the student model for large NFV systems. In the following, we first describe the architecture of MAE and DevNet individually, and then illustrate how they are integrated together in our proposed student model for performing anomaly detection.

MAE Architecture: MAE is a transformer-based Auto-encoder model that similarly to other transformer models considers the input data as a sequence of tokens (e.g., words of a sentence in NLP or patches of images in computer vision). In our case, metrics of each VNF ($vnf_t^j, j \in \{1, 2, ..., k\}$) are the k input tokens for our MAE model. To convert the input tokens to vectors of equal dimension d_{enc}, we use k linear projection layers with trainable weights (with input size n_j and output size d_{enc}) that transform each $vnf_t^j \in \mathbb{R}^{1 \times n_j}$ to $z_1^j \in \mathbb{R}^{1 \times d_{enc}}$, such that the input $x_t = \{vnf_t^1, vnf_t^2, ..., vnf_t^k\}$ is converted into $z_1(x_t) = \{z_1^1, z_1^2, ..., z_1^k\} \in \mathbb{R}^{k \times d_{enc}}$. In transformer models, positional encoding features [16] are added to the input so the model is informed of the order of tokens in the input sequence (in our case, the model would know which token is related to which one of the VNFs). The positional encoding features ($pos \in \mathbb{R}^{k \times d_{enc}}$) have the same dimension d_{enc} for each token, so after adding the positional encoding we have:

$$z_2(x_t) = z_1(x_t) + pos \tag{11}$$

$$z_2(x_t) \in \mathbb{R}^{k \times d_{enc}} \tag{12}$$

The idea for learning a very generalizable representation in MAE is to randomly mask (remove) a portion of the encoder's input data (a fixed number of the input tokens), and forcing the decoder to reconstruct the entire input data from the incomplete information that is encoded by the encoder. For the sake of simplicity, in our approach, we assume that only the metrics of one of the VNFs (one input token) is randomly selected to be masked from the encoder. However, all the following algorithms can be easily extended to cases where the metrics of more than one VNF are masked. So, we first randomly (with uniform distribution) select the number m from $\{1, 2, ..., k\}$, and remove the features related to the m-th VNF from z_2 to obtain z_3:

$$z_3(x_t, m) = \{z_2^1, z_2^2, ..., z_2^{m-1}, z_2^{m+1}, ..., z_2^k\} \tag{13}$$

$$z_3(x_t, m) \in \mathbb{R}^{(k-1) \times d_{enc}} \tag{14}$$

Now, z_3 is the input to the MAE's encoder. This encoder is a standard ViT encoder [16], which is a series of transformer blocks that transforms the input to a latent representation $z_4(x_t, m) \in \mathbb{R}^{(k-1) \times d_{enc}}$. Then, before feeding this latent representation to the decoder to reconstruct the original input, we need to concatenate it with a random trainable vector of dimension d_{enc}, called mask token [16], to inform the decoder that the information in the m-th position (metrics regarding the m-th VNF) is masked. Let's denote the mask token as M_{token}, then the output $z_5(x_t, m)$ will be the concatenation of $z_4(x_t) = \{z_4^1, z_4^2, ..., z_4^{k-1}\}$ and M_{token}:

$$z_5(x_t, m) = \{z_4^1, z_4^2, ..., z_4^{m-1}, M_{token}, z_4^m, ..., z_4^{k-1}\} \tag{15}$$

$$z_5(x_t, m) \in \mathbb{R}^{k \times d_{enc}} \tag{16}$$

Similar as for the encoder, we need to add positional encoding features to z_5 before feeding it to the decoder:

$$z_6(x_t, m) = z_5(x_t, m) + pos \tag{17}$$

$$z_6(x_t, m) \in \mathbb{R}^{k \times d_{enc}} \tag{18}$$

Now we use a single projection layer (with input size

d_{enc} and output size d_{dec}) to project each token to a new dimension d_{dec} to obtain $z_7(x_t, m) \in \mathbb{R}^{k \times d_{dec}}$. $z_7(x_t, m)$ will be the input to our decoder. The decoder is also a series of transformer blocks that transforms $z_7(x_t, m)$ to another representation $z_8(x_t, m) \in \mathbb{R}^{k \times d_{dec}}$. Since MAE's goal is to reconstruct the original input sample, we should also have a final linear projection layer (with input size $k \times d_{dec}$ and output size d) at the end of the decoder to project the decoder's output $z_8(x_t, m)$ to a vector of dimension d, denoted as $z_9(x_t, m)$ (unlike previously mentioned projection layers that were applied separately on each token, this final projection layer is applied once on the entire decoder's output):

$$z_9(x_t, m) = \{z_9^1, z_9^2, ..., z_9^k\} \tag{19}$$

$$z_9^j \in \mathbb{R}^{1 \times n_j} \tag{20}$$

$$z_9(x_t, m) \in \mathbb{R}^{1 \times d}, d = \sum_{j=1}^{k} n_j \tag{21}$$

The MAE is trained according to the following loss function, which is the mean squared error (MSE) of the masked VNF original metrics and those reconstructed by the decoder:

$$L_{MAE} = MSE(vnf_t^m, z_9^m) \tag{22}$$

DevNet Architecture: DevNet is a weakly-supervised anomaly detection method that can utilize a limited number of known anomalies to improve anomaly detection performance. DevNet's architecture is a simple neural network that learns a scalar anomaly score $\Phi(x)$ value from its input samples x. In the training of DevNet, anomaly scores of normal samples are forced to be close to a reference average, and anomaly scores of known anomalous samples are forced to deviate significantly from this average. To achieve this goal, the following loss function is used for training DevNet:

$$L_{Dev}(x) = \begin{cases} |\frac{\Phi(x) - \mu_R}{\sigma_R}|, & \text{if } x \text{ is normal} \\ \\ max(0, a - \frac{\Phi(x) - \mu_R}{\sigma_R}), & \text{if } x \text{ is anomalous} \end{cases} \tag{23}$$

Same as in [16], we assume that anomaly scores of normal samples have a standard normal distribution $F : N(0, 1)$, and for training a batch of training samples, we draw l observations from this distribution: $(r_1, r_2, ..., r_l)$. Then, the reference average is calculated based on these l drawn observations: $\mu_R = \frac{1}{l} \sum_{i=1}^{l} r_i$ and $\sigma_R^2 = \frac{1}{l} \sum_{i=1}^{l} (r_i - \mu_R)^2$. Similar to the loss function in [16], our loss function pushes anomaly scores of normal samples in X_c to be near μ_R and requires anomaly scores of samples in $\tilde{X}_{anom}$ to deviate from μ_R with at least $a > 0$ confidence level. In our experiments, we chose $a = 5$ to ensure significant deviation from μ_R for our anomalous samples. Moreover, for creating a batch of training samples with size β, we select $\beta/2$ samples from X_c and $\beta/2$ samples from $\tilde{X}_{anom}$. In the end, based on the loss function, parameters of the DevNet are optimized by performing a gradient descent step.

Integrating MAE with DevNet: In our proposed student model depicted in Fig. 1, we integrate MAE with DevNet and train the entire model on X_{new} in an end-to-end fashion. More specifically, instead of feeding the input samples directly to the DevNet model, the samples first go through the MAE, and then, the latent features learned by the MAE encoder alongside reconstruction error features calculated based on the difference between the input and output of MAE are fed to DevNet for calculating the anomaly scores of the samples. So, the new input of DevNet, $x'(x_t, m)$, is:

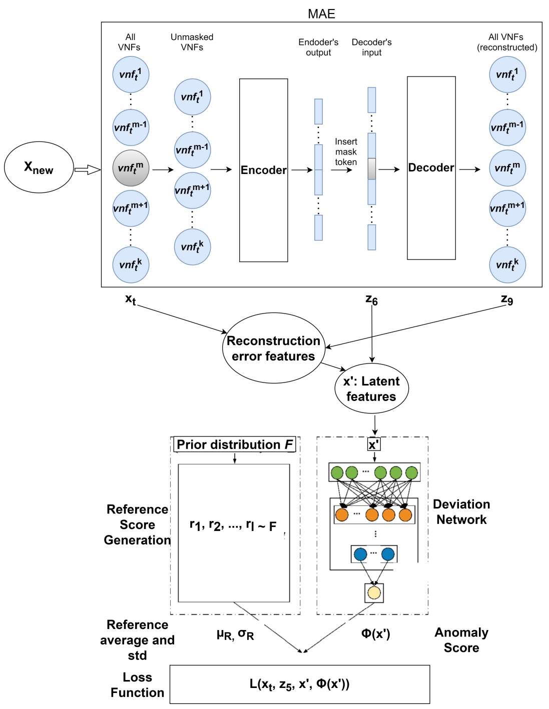

Fig. 1. The proposed student model to be trained on X_{new}. The latent features (low-dimensional representation and reconstruction error features) are extracted from the input by the MAE and are fed to the Deviation Network. Then, the anomaly score output of the Deviation Network alongside average anomaly score of some normal samples (μ_R) that is calculated according to a prior distribution F are fed to the loss function for end-to-end training of the whole model.

$$x'(x_t, m) = \{z_6(x_t, m), rec_{err}(x_t, m)\} \in \mathbb{R}^{1 \times (k \times d_{enc} + k)} \tag{24}$$

$$rec_{err}(x_t, m) = \{||z_9^i - x_t^i||_2, i \in \{1, 2, ..., k\}\} \tag{25}$$

The student model is trained according to the following loss function, which is a combination of the loss functions of MAE and DevNet:

$$L(x_t) = \begin{cases} \alpha_1 \times L_{MAE} + |\frac{\Phi(x'(x_t, m)) - \mu_R}{\sigma_R}|, & \text{if } x_t \in X_c \\ \\ max(0, a - \frac{\Phi(x'(x_t, m)) - \mu_R}{\sigma_R}), & \text{if } x_t \in \tilde{X}_{anom} \end{cases} \tag{26}$$

Where $L_{MAE} = MSE(vnf_t^m, z_9^m)$, and $\alpha_1 > 0$ determines the effect of the two components of loss function for normal samples. At inference time, we calculate the average of $\Phi(x'(x_a, m))$ for a test sample x_a when m varies from 1 to k, and the test sample is considered as an anomaly if this average value exceeds a predefined threshold (e.g., $a/2$).

V. Anomaly Localization

After an anomaly is detected, localizing the VNF that is responsible for the anomalous behavior of the system is the next important step in fault management of NFV systems. In this paper, we assume the reasonable assumption that as the probability of multiple simultaneous failures is very small, the anomalous behavior originates only from one of the VNFs, and our localization objective is to pinpoint the corresponding VNF. We first present an anomaly localization algorithm called "Mask Permutation" that utilizes the outputs of the our anomaly detection model for different masking scenarios to determine the anomaly location (exclusive for our anomaly detection model MNSUAD). Furthermore, we propose two more generic algorithms for anomaly localization based on XAI methods that are applicable to any black-box ML-based anomaly detection model. All three algorithms perform the anomaly localization task in a fully-automated manner without requiring domain experts' intervention.

A. Localization with Mask Permutation

The goal of Mask Permutation is to observe the output of the detection model for different masking scenarios and determine the anomaly location based on the information provided by these different outputs. Let us assume x_a is a detected anomaly sample. If vnf^j is the anomaly location, we expect the following behavior from our detection model:

When metrics of vnf^j are masked: if metrics of vnf^j are masked, we would expect the reconstruction error for vnf^j to be high (big difference between predicted values and actual values of vnf^j's metrics). The reconstruction error can be calculated according to the following:

$$\Omega(x_a, j) = MSE(vnf_a^j, z_9^j(x_a, j)) \tag{27}$$

Moreover, since the metrics of the anomalous VNF are not given to the MAE, we would expect a relatively lower anomaly score when metrics of vnf^j are masked (we expect $\phi(x_a, j) = |\frac{\Phi(x'(x_a,j))-\mu_R}{\sigma_R}|$ to be lower relative to when the metrics of a VNF other than vnf^j are masked).

When metrics of vnf^j are not masked: Let us assume metrics of vnf^i are masked ($i \neq j$). Then, the anomaly score calculated by the detection model would be $\Phi(x'(x_a, i))$. Now, assume we replace the metrics of vnf^j (the anomalous VNF) with values that the MAE predicts for it when it is masked (i.e., $z_9^j(x_a, j)$) to create a synthetic sample $x_{syn}(j)$:

$$x_{syn}(j) = \{vnf_a^1, ..., vnf_a^{j-1}, z_9^j(x_a, j), vnf_a^{j+1}, ..., vnf_a^k\} \tag{28}$$

Since metrics' values of the anomalous vnf^j are replaced with predicted values $z_9^j(x_a, j)$, we expect the anomaly score of this synthetic sample to be lower than the anomaly score of the original sample when metrics of vnf^i are masked (i.e., we expect $|\frac{\Phi(x'(x_{syn}(j),i))-\mu_R}{\sigma_R}| \leq |\frac{\Phi(x'(x_a,i))-\mu_R}{\sigma_R}|$). We denote this difference as $\Delta\Phi(x_a, j, i)$:

$$\phi(x_a, i) = |\frac{\Phi(x'(x_a, i)) - \mu_R}{\sigma_R}| \tag{29}$$

$$\phi(x_{syn}(j), i) = |\frac{\Phi(x'(x_{syn}(j), i)) - \mu_R}{\sigma_R}| \tag{30}$$

$$\Delta\Phi(x_a, j, i) = \phi(x_a, i) - \phi(x_{syn}(j), i) \tag{31}$$

Based on these expectations, we define a global localization score (GLS) for each vnf^j and denote it as $G(j)$:

$$G(j) = \alpha_2 \times \Omega(x_a, j) - \phi(x_a, j) + \frac{\sum_{i \neq j} \Delta\Phi(x_a, j, i)}{k-1} \tag{32}$$

Where $\alpha_2 > 0$ adjusts the effect of the reconstruction error component of the GLS. The higher the $G(j)$ score is, the higher is the probability that vnf^j is the location of the system's anomalous behavior. We calculate $G(j)$ for all the k VNFs ($j \in \{1, 2, ..., k\}$) and choose the VNF with the highest GLS to be the anomaly location.

B. Localization with SHAP

The complete procedure of anomaly localization with the SHAP method [48] is presented in Algorithm 1. To determine the contribution of each feature to the decision of the anomaly detection model, SHAP gets the detected anomaly sample x_a, the anomaly detection model (e.g., MNSUAD), and a set of background input samples to explore the input space with. Giving the entire training samples as the background data to the SHAP method would result in a highly impractical execution time. A possible solution is to apply k-means on the training data and give the obtained centroids, as representatives of the training data, to the SHAP method. In our experiments, we applied k-means on X_{new} (e.g., with 50 clusters) and gave the corresponding centroids $Cents$ to the SHAP method as background data to achieve a reasonable execution time. $Shap_{x_a} \in \mathbb{R}^{1 \times d}$, the output of the SHAP method for the detected anomaly x_a, has a value for each feature that represents the effect of the feature on the detection model's output for this detected anomaly. In the next step, for each vnf^j, we separate elements of $Shap_{x_a}$ corresponding to the features of vnf^j and denote it as $Shap_{x_a}^j \in \mathbb{R}^{1 \times n_j}$. Finally, the anomaly location is chosen to be the VNF whose SHAP values ($Shap_{x_a}^j$) have the highest first norm. We have also considered a scaling factor $c_j \in C$ for each $Shap_{x_a}^j$ to avoid any potential biases towards/against some specific VNFs. For example, in our experiments, we chose $c_j = \frac{1}{\sqrt{n_j}}$ to avoid being biased towards the VNFs from which we collect a higher number of features (n_j being the number of features collected from vnf_j). Moreover, it is important to note that we chose the first norm instead of the second norm because it allows the algorithm to consider a higher number of features in localizing the anomaly, where the second norm might focus the algorithm on a few specific features (i.e., features with large SHAP values become too dominant in determining the anomaly location) and degrade the localization performance. The SHAP localization method can be applied to any ML-based anomaly detection model that calculates an anomaly score for any given data sample.

Algorithm 1 Anomaly Localization with SHAP

```
1: function ShapLocal($x_a, MNSUAD, Cents, C$)
2:     $Shap_{x_a} \leftarrow SHAP(x_a, MNSUAD, Cents)$
3:     $Shap^j_{x_a} \leftarrow$ elements of $Shap_{x_a}$ related to $vnf^j$
4:     $location \leftarrow argmax_j(c_j||Shap^j_{x_a}||_1)$
5:     return $location$
```

C. Localization with Cluster Permutation

SHAP is a general model-agnostic XAI method that is designed to be applicable to any ML task. For improving the accuracy and reducing the computational complexity of our localization method, we propose our own novel XAI algorithm (called Cluster Permutation) that is specifically designed for the task of anomaly localization but is still applicable to any anomaly detection model. The overall procedure of Cluster Permutation is presented in Algorithm 2. In this algorithm, to check whether vnf^j is the location of the detected anomaly $x_a = \{vnf^1_a, vnf^2_a, ..., vnf^k_a\}$, we first define the metrics related to vnf^j in x_a as $\overline{x_a(j)}$, and the remaining metrics in x_a as $\widehat{x_a(j)}$. We do the same separation on all the samples in X_c (a total of s samples) to obtain $\overline{X_c(j)}$ and $\widehat{X_c(j)}$. Then, by the K-Nearest Neighbors (KNN) algorithm, we find the indices of the nearest neighbors of $\widehat{x_a(j)}$ in the $\widehat{X_c(j)}$ dataset. These neighbors would be normal samples that resemble our detected anomaly sample when we are excluding metrics of vnf^j. Our intuition is that if vnf^j is the location of the anomaly, by replacing the current metrics of vnf^j in the detected anomaly with metrics related to vnf^j in normal neighbors, the new created sample (x^{mod}_a) would have a lower degree of anomalous behavior, and its anomaly score would be lower and closer to μ_R. For each vnf^j, we measure the average change in the anomaly score for all the neighbor samples, and the vnf^j that has the highest decrease in anomaly score when its metrics are replaced by normal neighbors' metrics is chosen as the location of the anomaly. However, if there is no decrease in the anomaly score for any of the VNFs or the decrease in the anomaly score is less than a threshold (Thr) that is given to the algorithm, the output of the algorithm is "undecided". So, in this case, we ran the ShapLocal algorithm (Algorithm 1) to determine the anomaly location. The Cluster Permutation method is also applicable to any ML-based anomaly detection model that that computes an anomaly score for a given data sample.

One important point is that even though X_c is much less contaminated than the original training data, it still has some degree of contamination, but in this algorithm, we are treating X_c as if it only includes normal samples. However, this issue would not be problematic if we choose K in the KNN algorithm large enough so that the obtained neighbors include enough normal samples for the algorithm to work properly.

Algorithm 2 Anomaly Localization with Cluster Permutation

```
1: function ClusterPer($x_a, X_c, MNSUAD, Thr$)
2:     $\Delta\Phi \leftarrow \{\}$
3:     for $j = 1$ to $k$ do
4:         $\overline{x_a(j)} := \{vnf^j_a\} \in \mathbb{R}^{1\times n_j}$
5:         $\widehat{x_a(j)} := (x_a \setminus \overline{x_a(j)}) \in \mathbb{R}^{1\times(d-n_j)}$
6:         $\overline{X_c(j)} = \{\overline{x_{c1}(j)}, \overline{x_{c2}(j)}, ..., \overline{x_{cs}(j)}\}$
7:         $\widehat{X_c(j)} = \{\widehat{x_{c1}(j)}, \widehat{x_{c2}(j)}, ..., \widehat{x_{cs}(j)}\}$
8:         Run KNN in $\widehat{X_c(j)}$ for $\widehat{x_a(j)}$
9:         Find nearest neighbors: $\widehat{X_{cp}(j)}, p \in \mathbb{NEIGHB}$
10:        $\Delta\phi \leftarrow 0$ , $c \leftarrow 0$
11:        for $p \in \mathbb{NEIGHB}$ do
12:            $x^{mod}_a \leftarrow \{vnf^1_a, ..., vnf^{j-1}_a, \overline{x_{cp}(j)}, ..., vnf^k_a\}$
13:            $\Phi(x_a) := \frac{1}{k}\sum_{m=1}^{k}\Phi(x'(x_a, m))$
14:            $\Phi(x^{mod}_a) := \frac{1}{k}\sum_{m=1}^{k}\Phi(x'(x^{mod}_a, m))$
15:            $\Delta \leftarrow |\frac{\Phi(x_a)-\mu_R}{\sigma_R}| - |\frac{\Phi(x^{mod}_a)-\mu_R}{\sigma_R}|$
16:            if $\Delta > 0$ then
17:                $\Delta\phi \leftarrow \Delta\phi + \Delta$
18:                $c \leftarrow c + 1$
19:        if $c > 0$ then
20:            $\Delta\Phi.append(\frac{\Delta\Phi}{c})$
21:        else
22:            $\Delta\Phi.append(0)$
23:    $location \leftarrow argmax(\Delta\Phi)$
24:    $\Delta\Phi_{max} \leftarrow max(\Delta\Phi)$
25:    if ($\Delta\Phi_{max} > Thr$) then
26:        $output \leftarrow location$
27:    else
28:        $output \leftarrow ShapLocal(x_a)$
29:    return $output$
```

VI. Experimental Results

In this section, we first introduce the three datasets on which we evaluated our anomaly detection and localization methods. Then, we describe the-state-of-the-art approaches that are compared with our proposed methods. Following this, we conduct a detailed examination and analysis of the results obtained from applying our methods to detect and localize anomalies within these datasets. Additionally, we compare our student model with state-of-the-art weakly-supervised methods and our MNSUAD method with fully supervised methods in terms of generalization capability.

A. Datasets

ITU Dataset: Our first dataset is from the "ITU AI/ML in 5G" challenge [49]. It was generated in an NFV-based test environment that simulates a 5G IP core network. The target topology of the NFV testbed is shown in Fig. 2a and consists of 5 VNFs: two IP core nodes (TR-01 and TR-02), two internet gateway routers (IntGW-01 and IntGW-01), and a router reflector (RR-01), each hosted on a different Virtual Machine (VM). Various performance metrics, such as CPU utilization and network incoming/outgoing packet rates, are collected from each VNF per minute. For evaluation of the anomaly-detection mechanisms, the following fault scenarios are injected to one of the VNFs periodically: 1) node failure, i.e., an unplanned reboot of a VNF. 2) interface failure, i.e., a failure that causes an interface to be down, and 3) packet loss/delay, i.e., an event that causes packet loss/delay on an interface. We label each faulty instance according to the location of the fault (1:5, the VNF to which the fault is injected), and that would be the target that our localization algorithms should predict. A well-structured version of this dataset can be found in [50]. For this dataset, the training data includes 3870 normal samples, and the test data includes 3505 normal samples and 1112 anomalies. For creating a certain level of contamination in the training data, we choose some anomalous samples at random from a set that includes an equal number of different types of anomalies and add those anomalies to the training data. When extracting pseudo-labeled anomalies from this training data according to the procedure in Section IV.B, we observed that, as expected, the number of extracted pseudo-labeled anomalies was larger for higher contamination rates. More specifically, the number of extracted pseudo-labeled anomalies (on average for multiple runs) was 25, 41, 57, 65, and 72 for 1%, 2%, 3%, 4%, and 5% contamination rates, respectively.

MEC Dataset: Our second dataset is from our experimental NFV testbed depicted in Fig. 2b, and consists of 4 open-source VNFs: a Firewall (iptables [51]), an intrusion detection System (Suricata [52]), a deep packet inspector (nDPI [53]), and a flow monitor (ntopng [54]). We have adopted the topology in Fig. 2b from [24] and implemented it on the SAVI testbed [55], where each of the VNFs is hosted on a different VM. We used Apache Bench for traffic generation in the testbed. We have collected 61 resource-related metrics (CPU, Disk, memory, and network) from all the VNFs every 5 seconds (see [24] for a complete list of collected metrics). We injected one of the following faults to one of the VNFs periodically to generate faulty instances to evaluate our anomaly-detection techniques: 1) *CPU stress* by the stress-ng [56] tool that increases the CPU usage in the VM, 2) *disk stress* by the stress-ng [56] tool that increases the disk usage in the VM, and 3) *network stress* by the tc [57] tool where network delay of one of the interfaces in a VM increases. For this dataset, the training data includes 3500 normal samples, and the test data includes 1500 normal samples and 200 anomalous samples. Similarly, we extract pseudo-labeled anomalies from the training data of this dataset according to the procedure in Section IV.B. The number of extracted pseudo-labeled anomalies (on average for multiple runs) was 28, 52, 72, 84, and 89 for 1%, 2%, 3%, 4%, and 5% contamination rates, respectively.

IMS Dataset: This dataset is collected by [18] from the ClearWater project, which is an NFV-based open source implementation of an IMS for cloud platforms. The IMS consists of the ten components depicted in Fig. 2c, each deployed on a docker container. The dataset contains the performance metrics of the three most important components, namely Bono, Sprout, and Homestead, which are responsible for controlling sessions initiated by users. The performance metrics are collected from the containers every 5 seconds. For generating faulty data instances, they inject CPU fault, Memory fault, or i/o fault randomly to one of these three components (at each fault scenario, one of these fault types is injected to one of the three main components). The training data here includes 480 normal samples and the test data has 120 normal samples and 700 anomalous samples. Similarly, we extract pseudo-labeled anomalies from the training data of this dataset according to the procedure in Section IV.B. The

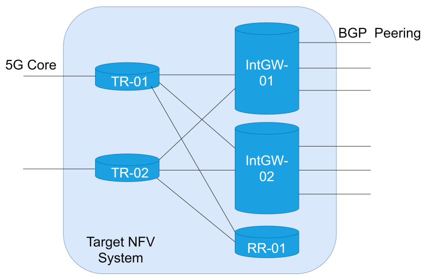

(a)

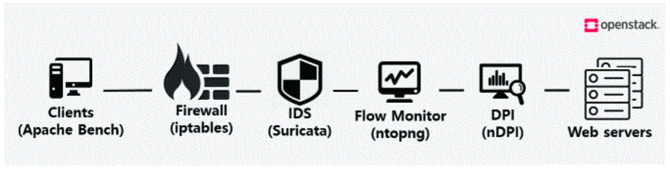

(b)

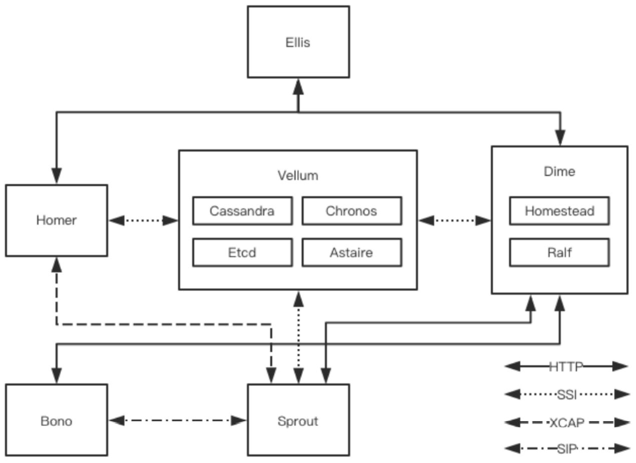

(c)

Fig. 2. NFV system of (a) ITU Dataset, (b) MEC Dataset [24], and (c) IMS Dataset [6].

number of extracted pseudo-labeled anomalies (on average for multiple runs) was 3, 6, 11, 14, and 16 for 1%, 2%, 3%, 4%, and 5% contamination rates, respectively.

1) Data Preprocessing

We perform the necessary data preprocessing tasks before feeding the data to the ML models, including replacing the accumulative values (e.g., number of packets sent) with their numeric difference, data normalization due to the different dynamic ranges of the collected metrics, metric selection, etc. The compared approaches were evaluated on a server with 2x20 core Intel Xeon Silver 4114 2.20GHz CPU, 187 GB memory, and NVIDIA Tesla P40 GPU.

B. Compared Approaches

Baseline: The baseline approach used to compare our detection approach with is the Autoencoder-based anomaly-detection algorithm in [6] and [11], where the Autoencoder is trained on only normal samples and then based on the overall reconstruction error of the Autoencoder, anomalies are separated from normal samples in the test data. Since [6] and [11] have worked with different datasets that are not publicly available, we have designed the best Autoencoder architecture for our datasets by trying different architectures,

TABLE I
Anomaly-detection results of different methods on contaminated training data with the contamination percentage (δ) varying from 0% to 5%

δ	ITU Dataset											
	Baseline			DAGMM			MSCRED			MNSUAD (ours)		
	Pr.	Re.	F1	Pr.	Re.	F1	Pr.	Re.	F1	Pr.	Re.	F1
0	80.8	46.6	58.9	**83.3**	**82.1**	**82.7**	76.4	62.2	68.4	-	-	-
1	77.6	31.4	44.8	80.1	80.2	80.1	71.5	55.9	62.3	**84.8**	**84.3**	**84.5**
2	76.9	31.1	44.5	79.3	78.9	79.1	68.6	49.3	57.3	**86.3**	**85.0**	**85.6**
3	76.1	30.0	43.0	75.8	74.8	75.3	57.7	42.1	48.6	**86.7**	**85.3**	**86.0**
4	75.8	29.5	42.6	73.5	72.6	72.9	41.5	32.6	36.5	**87.7**	**85.9**	**86.8**
5	74.5	29.2	42.0	71.8	71.7	71.7	27.8	24.3	25.9	**87.1**	**85.6**	**86.3**

δ	MEC Dataset												IMS Dataset											
	Baseline			DAGMM			MSCRED			MNSUAD (ours)			Baseline			DAGMM			MSCRED			MNSUAD (ours)		
	Pr.	Re.	F1	Pr.	Re.	F1	Pr.	Re.	F1	Pr.	Re.	F1	Pr.	Re.	F1	Pr.	Re.	F1	Pr.	Re.	F1	Pr.	Re.	F1
0	83.4	78.5	80.9	**85.8**	**83.7**	**84.7**	76.2	73.3	74.7	-	-	-	98.8	97.5	98.1	98.1	96.9	97.5	**100**	**100**	**100**	-	-	-
1	80.3	71.2	75.5	82.1	78.8	80.4	65.6	62.7	64.0	**93.0**	**89.7**	**91.3**	74.8	74.1	74.4	84.8	81.4	83.1	65.7	64.3	65.0	**95.1**	**93.4**	**94.2**
2	78.9	64.1	70.7	77.3	75.2	76.2	49.3	48.8	49.1	**94.2**	**93.5**	**93.8**	68.6	67.1	67.8	80.1	78.3	79.2	59.1	58.2	58.6	**96.4**	**95.2**	**95.8**
3	77.2	60.9	68.1	74.5	73.6	74.1	41.2	38.7	39.9	**94.8**	**93.2**	**94.0**	64.2	62.3	63.2	78.2	75.4	76.8	52.4	51.0	51.7	**96.6**	**95.3**	**95.9**
4	70.8	59.5	64.6	73.6	71.8	72.7	33.9	30.5	32.1	**95.3**	**93.5**	**94.4**	54.9	50.1	52.4	73.5	71.6	72.5	47.1	47.0	47.1	**96.6**	**95.5**	**96.1**
5	66.7	52.6	58.8	70.3	69.9	70.1	20.3	19.7	20.0	**95.2**	**94.0**	**94.6**	50.8	47.3	49.0	72.7	70.9	71.8	42.4	42.2	42.3	**96.5**	**95.3**	**95.9**

from very shallow to very deep, to reach the best possible outcome for the Baseline. Moreover, similar to [11], we added L2-regularization to the Autoencoder network to improve the model's robustness against contamination in the training data. For the baseline localization approach, we implemented the conventional method where the VNF whose features have been reconstructed more poorly is chosen as the location of the fault (Let $x'_t = \{vnf'^1_t, vnf'^2_t, ..., vnf'^k_t\}$ be the reconstructed output of a vanilla Autoencoder for the input sample $x_t = \{vnf^1_t, vnf^2_t, ..., vnf^k_t\}$. We calculate the reconstruction error $||vnf'^j_t - vnf^j_t||_2$ for each vnf^j, and choose the VNF with the highest reconstruction error as the fault location).

DAGMM: Our teacher model, DAGMM [13], trained on the whole training data, is another compared approach. DAGMM has shown to be robust against contamination in the training data to some extent since it performs density estimation on features extracted from its Autoencoder. Therefore, it is a good choice to be compared with our approach when dealing with contaminated training data. The localization task here is the same as the Baseline.

MSCRED: Multi-Scale Convolutional Recurrent Encoder-Decoder (MSCRED) was proposed in [45] for unsupervised anomaly detection and localization (diagnosis) in multivariate time series data. In this approach, inter-correlation between different metrics is calculated with different temporal window sizes, and a Recurrent Encoder-Decoder DL model is trained to construct these inter-correlations for normal instances. Then, anomaly-detection and localization tasks are performed based on the reconstruction errors of these inter-correlations values.

Our Proposed Methods: MNSUAD is our proposed anomaly-detection solution described in Section IV. SHAP (Algorithm 1), ClusterPer (Algorithm 2), and MaskPer (Section V.A) are our proposed anomaly-localization approaches that utilize MNSUAD as their detection model.

C. Detection Results

The performance metrics for anomaly detection (namely, Precision, Recall, and F1-score) of different approaches are shown in Table I. In the first row of Table I, we report the detection performance metrics when there is no contamination in the training data ($\delta = 0\%$), so we can clearly observe the effect of contamination on these approaches in the next experiments. In the next rows of Table I, we change the contamination percentage (δ) in the training data from 1% to 5% and report the detection performance. We can see that contamination in the training data significantly degrades the performance of Baseline, MSCRED, and DAGMM, and this degradation becomes more severe as δ increases. Also, in all datasets, DAGMM has a better average performance than Baseline and MSCRED (especially in the ITU dataset), and its performance degrades less significantly compared to the Baseline and MSCRED as δ increases; therefore, DAGMM is confirmed to be an excellent choice as the teacher model in our approach.

Moreover, our detection approach MNSUAD has a better performance than DAGMM, MSCRED, and Baseline when δ is 1%, and, unlike the other approaches, the detection performance of MNSUAD improves when δ increases up to 5% since it takes advantage of the extracted pseudo-labeled anomalies in the contaminated training data. More specifically, increasing δ (percentage of anomalous samples) in the training data has one negative effect and one positive effect on MNSUAD's performance. The negative effect is that as δ increases, the performance of MNSUAD's teacher model (DAGMM) degrades. The positive effect is that MNSUAD extracts more pseudo-labeled anomalies when δ is higher. In our experiments, when we increase δ up to 5%, the positive effect seems to be more dominating than the negative effect most of the time; therefore, the overall performance of MNSUAD usually becomes better for higher contamination percentages in the training data.

However, we expect that after a certain level of contamination, the degradation in the teacher model's performance (the negative effect) becomes significant enough to decrease MNSUAD's overall performance. For example, when we increased δ to 8%, the teacher model's F1-score declined to 65.4%, 64.1%, and 67.5% in the ITU, MEC, and IMS datasets, respectively. Consequently, MNSUAD's F1-score degraded to 81.1%, 88.5%, and 91.4%; so, the MNSUAD's F1-scores with 8% contamination become much lower than the case where δ

was 5% in the three datasets. For very high contamination levels in the training data, Active Learning [58] approaches that label the data with the help of domain experts might be more suitable.

D. Comparison of Different Weakly-supervised Learning Anomaly Detection Methods

In our experiments so far, our proposed MNSUAD method has been the only approach that is trained on X_{new}, and all the other compared approaches were trained on the original contaminated training dataset . To show that the performance improvement achieved by MNSUAD is not just due to cleaning the contaminated dataset, in this section, we compare our student model in MNSUAD with other state-of-the-art weakly-supervised anomaly detection methods when they are also trained on the newly obtained dataset X_{new}. We implemented the following weakly-supervised anomaly detection methods for comparison with our student model:

DevNet [16]: As we described earlier, our student model integrates DevNet with MAE for a better feature encoding. In this algorithm, we directly apply the DevNet on the raw input samples. Comparing the result of this algorithm with our student model can better illustrate the effectiveness of using an MAE for learning a richer feature representation in MNSUAD.

V-DevNet [33]: V-DevNet is a modified version of DevNet, where the reference scores used in the deviation loss of DevNet are calculated by a Variational Auto-encoder (VAE), instead of generating them according to a prior probability.

D-SAD [34]: In this algorithm, a neural network is trained to transform the input space to a lower-dimensional output space with the goal that the output of unlabeled samples should be as close as possible to a predetermined center point, while maximizing the quadratic distance of known anomaly samples from this multi-dimensional center point. This algorithm can be considered as an extension of the Deep one-class classification method proposed in [59].

PRO [35]: In this algorithm, anomaly detection is reformulated as a pairwise relation prediction task in order to take advantage of a few available labeled anomaly samples. More specifically, the algorithm tries to train a supervised learning method on unordered random instance pairs labeled as anomaly-anomaly, anomaly-unlabeled, or unlabeled-unlabeled.

NSUAD [19]: NSUAD is the proposed algorithm in our previous work, where DevNet is integrated with a vanilla auto-encoder to perform the anomaly detection task.

The anomaly detection performance of the mentioned weakly-supervised methods (namely, Precision, Recall, and F1-score) are presented in Table II. We can see that DevNet and V-DevNet have a very similar performance, so we can conclude that calculating the reference scores through a data-driven approach (e.g., VAE) instead of a prior distribution has no significant effect on the anomaly detection performance. Among the compared approaches, PRO has the lowest average F1-score. This is expected as we only have access to pseudo-labeled anomalies rather than accurately labeled data samples. Thus, generating different instance pairs from the pseudo-labeled pairs (anomaly-anomaly, anomaly-unlabeled) would intensify the inaccuracies of pseudo-labels and would lead to a poor performance as we can see from our experiments. Moreover, results of Table II show that D-SAD has a slightly better performance than DevNet and V-DevNet in all the datasets since it projects the input space into a multi-dimensional outer space close to a center point as opposed to DevNet and V-DevNet that transform the input space into a single anomaly score value as the output space. Finally, we can see that the MNSUAD and NSUAD methods, which learn the anomalous behavior from a latent space pre-processed by an auto-encoder architecture instead of learning it directly from the input samples, have the best performance compared to the other methods. The pre-processing in NSUAD is done by a vanilla auto-encoder while MSUAD performs the pre-processing through an MAE that as discussed earlier leads to learning a more generalizable feature representation. Our experiments confirm this intuition as the results show that on average, MNSUAD has a 1.7%, 3.7%, 4.3% better F1-score than NSUAD in the ITU dataset, MEC dataset, and IMS dataset, respectively. It is important to note that for lower contamination rates (and consequently fewer pseudo-labeled anomalies in the dataset), the difference between the performance of MNSUAD and NSUAD is more significant compared to when the contamination rate is higher. We believe the reason is that the MAE in MNSUAD learns a more generalizable representation compared to the vanilla Autoencoder in NSUAD, and thus, MNSUAD can achieve a high performance even with very few labeled anomalies, while NSUAD requires more labeled anomalies to reach its highest performance.

E. Comparison with Supervised Methods in terms of Generalization Capability

We mentioned that the main drawback of supervised anomaly detection methods is that they require abundant labeled faulty data to achieve a good performance, which is a scarce resource and would need domain experts to annotate numerous logs of anomalous scenarios. In this section, through a set of experiments, we illustrate another important disadvantage of supervised methods, which is the problem that they are restricted to the specific failure scenarios that exist in their training data and do not generalize to failure scenarios unseen during training. However, in traditional unsupervised anomaly detection methods, where training is only performed on normal samples, the model is naturally not specialized for some specific failure cases and can detect any anomalous behavior that deviates from the learned normal patterns. Our goal in this section is to show that unlike supervised methods, our proposed weakly-supervised student model for anomaly detection (that takes advantage of a few pseudo-labeled anomaly samples) is generalizable to fault scenarios unseen during training and has a similar behavior to traditional unsupervised approaches in this regard.

To compare the generalization capability of our proposed method with supervised learning approaches, we have conducted the following experiments on the ITU dataset described in Section VI.A. Let X_U denote the contaminated unlabeled training dataset (from the ITU dataset) that has 3870 normal

TABLE II
Anomaly-detection results of different weakly-supervised methods trained on X_{new} with the contamination percentage (δ) varying from 0% to 5%

δ	ITU Dataset																	
	DevNet			V-DevNet			D-SAD			PRO			NSUAD (ours)			MNSUAD (ours)		
	Pr.	Re.	F1	Pr.	Re.	F1	Pr.	Re.	F1	Pr.	Re.	F1	Pr.	Re.	F1	Pr.	Re.	F1
1	80.4	78.5	79.4	80.5	78.7	79.6	81.5	79.2	80.3	73.4	75.5	74.4	82.7	81.6	82.1	**84.8**	**84.3**	**84.5**
2	82.2	81.1	81.6	82.2	81.3	81.7	82.9	81.6	82.2	77.9	78.6	78.2	84.1	83.5	83.8	**86.3**	**85.0**	**85.6**
3	83.7	82.0	82.8	83.6	82.0	82.8	84.4	82.5	83.4	78.4	79.1	78.7	85.4	83.8	84.6	**86.7**	**85.3**	**86.0**
4	85.2	83.6	84.4	85.1	83.5	84.3	85.9	84.0	84.9	79.3	80.0	79.6	86.1	84.4	85.2	**87.7**	**85.9**	**86.8**
5	85.8	84.1	85.0	85.8	84.2	85.0	86.4	84.8	85.6	79.2	79.8	79.5	86.5	84.4	85.4	**87.1**	**85.6**	**86.3**
δ	MEC Dataset																	
	DevNet			V-DevNet			D-SAD			PRO			NSUAD (ours)			MNSUAD (ours)		
	Pr.	Re.	F1	Pr.	Re.	F1	Pr.	Re.	F1	Pr.	Re.	F1	Pr.	Re.	F1	Pr.	Re.	F1
1	82.8	82.1	82.5	82.7	82.1	82.4	83.0	82.6	82.8	66.5	66.3	66.4	86.1	83.5	84.8	**93.0**	**89.7**	**91.3**
2	85.2	84.3	84.7	85.1	84.3	84.7	87.3	86.5	86.9	72.1	72.2	72.2	90.4	87.1	88.7	**94.2**	**93.5**	**93.8**
3	89.6	87.8	88.7	89.6	87.8	88.7	90.8	90.0	90.4	78.4	78.2	78.3	92.7	90.5	91.6	**94.8**	**93.2**	**94.0**
4	91.2	90.4	90.8	91.3	90.4	90.9	92.6	91.3	91.9	79.2	79.5	79.3	93.2	91.1	92.1	**95.3**	**93.5**	**94.4**
5	91.6	91.0	91.3	91.7	91.2	91.4	92.5	91.4	91.9	78.5	78.4	78.5	93.1	91.4	92.2	**95.2**	**94.0**	**94.6**
δ	IMS Dataset																	
	DevNet			V-DevNet			D-SAD			PRO			NSUAD (ours)			MNSUAD (ours)		
	Pr.	Re.	F1	Pr.	Re.	F1	Pr.	Re.	F1	Pr.	Re.	F1	Pr.	Re.	F1	Pr.	Re.	F1
1	87.8	87.3	87.5	87.8	87.4	87.6	88.2	87.6	87.9	81.3	81.0	81.2	90.3	89.1	89.7	**95.1**	**93.4**	**94.2**
2	89.4	88.7	89.0	89.5	88.7	89.1	89.6	88.5	89.0	88.5	88.6	88.5	91.6	90.7	91.1	**96.4**	**95.2**	**95.8**
3	90.7	89.6	90.1	90.6	89.5	90.0	91.5	90.4	91.0	89.2	89.2	89.2	92.1	91.0	91.5	**96.6**	**95.3**	**95.9**
4	91.6	90.7	91.1	91.5	90.6	90.9	92.0	91.1	91.6	90.2	90.1	90.2	93.0	91.5	92.2	**96.6**	**95.5**	**96.1**
5	91.6	90.5	91.0	91.6	90.4	91.0	92.2	91.2	91.7	89.8	89.5	89.7	92.7	91.5	92.1	**96.5**	**95.3**	**95.9**

samples, 50 samples of node down (ND) failure, 50 samples of interface down (ID) failure, 50 samples of packet loss (PL) failure, and 50 samples of packet delay (PD) failure. So, X_U has a total of 200 failure samples, and its contamination rate is around 5%. On the other hand, let X_L denote the fully labeled training dataset that includes 3870 normal samples, 54 samples of ND failure, 233 samples of ID failure, 762 samples of PL failure, and 763 samples of PD failure. We define $X_L^{(ND-\nu)}$ as a subset of dataset X_L, where ν percent of ND failure samples are removed from X_L. For example, $X_L^{(ND-50)}$ would only have 27 samples of ND failure, and $X_L^{(ND-100)}$ would have no samples of ND failure. $X_L^{(ID-\nu)}$, $X_L^{(PL-\nu)}$, and $X_L^{(PD-\nu)}$ are defined in a similar way. Moreover, $X_U^{(ND-100)}$, $X_U^{(ID-100)}$, $X_U^{(PL-100)}$, and $X_U^{(PD-100)}$ would be the same as X_U but without any samples of ND, ID, PL, and PD failure, respectively. For each of these training datasets, we create a corresponding test dataset that only consists of anomalous samples of the missing failure scenario. For example, the test data for the training datasets $X_L^{(ND-\nu)}$ and $X_U^{(ND-100)}$ would be denoted as $T^{(ND)}$ that only consists of samples of ND failure. In our experiments, $T^{(ND)}$ has 100 samples of ND fault samples, $T^{(ID)}$ has 100 samples of ID fault samples, $T^{(PL)}$ has 100 samples of PL fault samples, and $T^{(PD)}$ has 100 samples of PD fault samples. We created the test datasets in this way because we are interested to see whether different methods are capable of detecting failure scenarios for which only very few samples (or even no samples) of them exist in the training data.

We trained Random Forest (RF) models as a supervised method on different subsets of the labeled dataset X_L (e.g., $X_L^{(ND-\nu)}$, $X_L^{(ID-\nu)}$, etc.) for different values of ν. Here, the RF model performs anomaly detection as a binary classification problem, similar to [24]. In Fig. 3(a), we have reported the obtained Recall score (the percentage of correctly detected anomalies to the total number of anomalies) of each RF model on its corresponding test dataset when the value of ν changes from 0 to 100. In Fig. 3(b), we have reported the Recall score of our proposed MNSUAD method when it is trained on different subsets of X_U. It is important to clarify that the performance of an RF model/MNSUAD trained on $X_L^{(ND-\nu)}$/$X_U^{(ND-100)}$ is reported on its corresponding test dataset $T^{(ND)}$ (this is true for other failure scenarios, too).

Fig. 3(a) shows that as we decrease the number of samples of a specific scenario in the labeled training data (increasing the value of ν), the ability of the supervised RF model to detect the samples of that failure case degrades significantly. For example, the Recall score of RF when trained on X_L is 87.0% on the $T^{(PL)}$ test set, but its Recall decreases to 75.6% and 68.8% when it's trained on $X_L^{(PL-90)}$ and $X_L^{(PL-100)}$, respectively. We can observe a similar decrease in the Recall score of RF for the other three failure scenarios, too. However, from Fig. 3(b), we can see that excluding all samples of a particular failure scenario from the unlabeled training dataset X_U has an insignificant effect on the performance of our MNSUAD method (for example, Recall score of MNSUAD on test data $T^{(PL)}$ when it is trained on X_U and $X_U^{(PL-100)}$ is almost the same value). This is due to the fact that the student model of MNSUAD only utilizes the pseudo-labeled samples to boost the performance, and does not need samples from all the considered failure scenarios. These results show that our MNSUAD is much more generalizable to unseen fault cases compared to supervised learning approaches. We reported the results of these experiments only for the ITU dataset as a case study, but similar results were obtained when we conducted similar experiments on the other two datasets. Finally, it is important to mention that we performed our

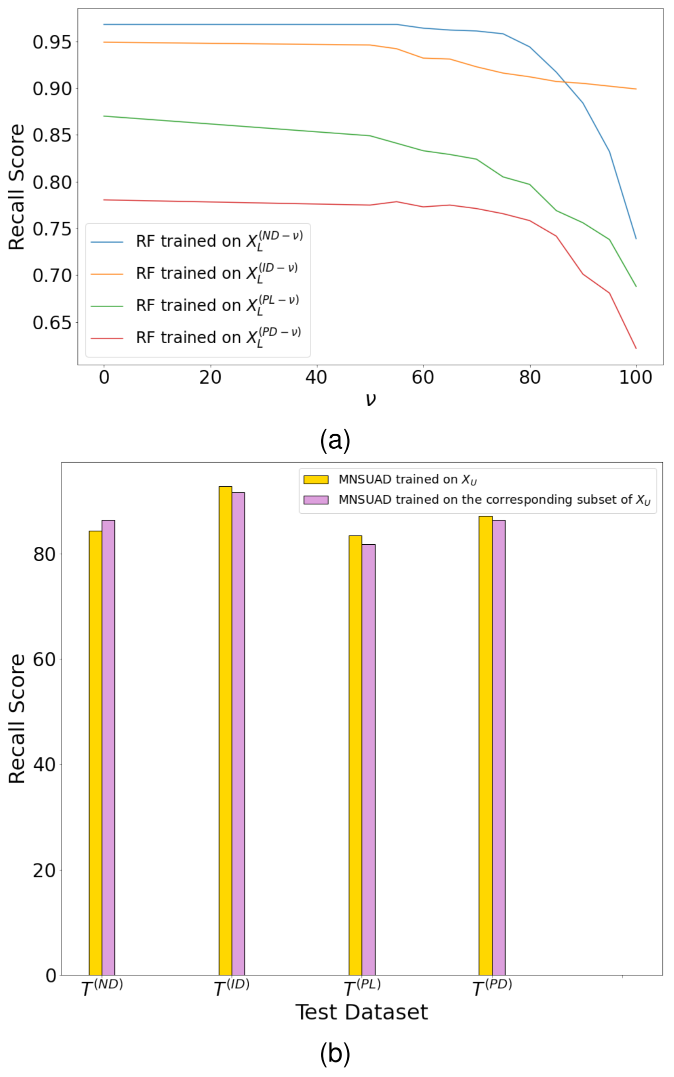

Fig. 3. The Recall scores of RF models trained on different subsets of X_L are shown in (a) when the value of ν changes from 0 to 100. (b) shows the Recall score of our MNSUAD method when it's trained on X_U compared to when its trained on one of the following datasets: $X_U^{(ND-100)}$, $X_U^{(ID-100)}$, $X_U^{(PL-100)}$, or $X_U^{(PD-100)}$.

experiments for different supervised learning methods, including Gradient Boosting Machine, Extreme Gradient Boosting, Deep Learning (Multilayer Perceptron), and RF. However, we only reported the performance of RF since it had the best performance among the supervised learning methods.

F. Localization Results

The performance metrics for anomaly localization (namely, Precision, Recall, F1-score, number of truly detected anomalies in the detection phase, and average execution time) of different approaches for the detected anomalies in the three datasets are shown in Table III. As discussed, the localization methods use a detection model for their process and localize the anomalies that are detected by that detection model. MNSUAD is the detection model for SHAP, ClusterPer, and MaskPer localization methods (with a training data that is 5% contaminated), and the detection models for the other localization methods are the same as their names according to Section VI.B. Therefore, the number of truly detected

TABLE III
Anomaly localization results of the compared approaches

ITU Dataset					
Method	Pr.	Re.	F1	#Anom.	Time(ms)
Baseline	62.4	65.1	62.7	516	**12**
DAGMM	58.3	58.2	58.2	913	13
MSCRED	73.6	73.4	73.4	698	17
SHAP (ours)	87.6	87.5	87.4	951	108
ClusterPer (ours)	92.5	92.5	92.5	951	37
MaskPer (ours)	**96.2**	**96.0**	**96.2**	951	22
MEC Dataset					
Method	Pr.	Re.	F1	#Anom.	Time(ms)
Baseline	73.3	73.1	73.2	157	**9**
DAGMM	64.2	64.4	64.2	167	**9**
MSCRED	78.5	78.6	78.5	110	12
SHAP (ours)	84.5	84.3	84.4	188	97
ClusterPer (ours)	93.2	93.1	93.1	188	22
MaskPer (ours)	**94.4**	**93.0**	**93.7**	188	20
IMS Dataset					
Method	Pr.	Re.	F1	#Anom.	Time(ms)
Baseline	61.4	61.7	61.6	682	**12**
DAGMM	57.3	57.5	57.5	678	**12**
MSCRED	74.6	73.5	74.2	700	15
SHAP (ours)	79.3	79.2	79.2	667	114
ClusterPer (ours)	84.3	84.2	84.2	667	32
MaskPer (ours)	**87.7**	**87.8**	**87.8**	667	25

anomalies is different for different approaches. According to the results of Table III, our SHAP and ClusterPer methods outperforms Baseline, MSCRED, and DAGMM in all datasets despite having more detected anomalies. Moreover, we can see that the MaskPer method that takes advantage of the output of the detection model for all the masking scenarios of the detected anomaly has achieved the highest F1-score on all the three datasets. We can also observe from these experiments that Baseline has the lowest average execution time in the datasets since its procedure is a simple analysis of the reconstruction error of different features, while SHAP has the highest execution time due to its relatively complex calculations. Since ClusterPer only needs to perform the SHAP calulation if its initial result is "undecided", its average execution time is much lower than the SHAP method. As MaskPer's procedure simply includes calculating the output of the detection model a few times for the detected anomaly sample, its average execution time is even lower than ClusterPer. So, we can conclude that the significant improvement in F1-score obtained by ClusterPer and MaskPer comes at the price of only a slight increase in the execution time.

VII. Conclusion

We proposed an unsupervised method for anomaly detection in NFV systems that is robust against training-data contamination up to a certain percentage and can also leverage the contamination to improve anomaly-detection performance, unlike state-of-the-art unsupervised approaches whose performances degrade when the training data is contaminated. Moreover, we described how utilizing the information provided by the MAE in our detection model can help to achieve a high accuracy in the anomaly localization task. Through a comprehensive experimental analysis on three datasets from different NFV systems, we showed that in terms of F1-score, our proposed solutions outperform other state-of-the-art unsupervised methods by up to 24% and 22% in anomaly-detection and localization tasks, respectively.

For future work, we plan to work on further improving the generalization of our detection/localization models, evaluating their applicability on larger and more complex datasets. We also plan to investigate how we can identify of the type of faults in an unsupervised manner in the NFV system.

Acknowledgement: This work was supported in part by Rogers Communications Canada Inc. and in part by a Mitacs Accelerate Grant.

References

[1] R. Mijumbi, J. Serrat, J.-L. Gorricho, N. Bouten, F. De Turck, and R. Boutaba, "Network function virtualization: State-of-the-art and research challenges," *IEEE Communications surveys & tutorials*, vol. 18, no. 1, pp. 236–262, 2015.

[2] B. Yi, X. Wang, K. Li, M. Huang *et al.*, "A comprehensive survey of network function virtualization," *Computer Networks*, vol. 133, pp. 212–262, 2018.

[3] B. Han, V. Gopalakrishnan, L. Ji, and S. Lee, "Network function virtualization: Challenges and opportunities for innovations," *IEEE Communications Magazine*, vol. 53, no. 2, pp. 90–97, 2015.

[4] B. Han, V. Gopalakrishnan, G. Kathirvel, and A. Shaikh, "On the resiliency of virtual network functions," *IEEE Communications Magazine*, vol. 55, no. 7, pp. 152–157, 2017.

[5] J. Nam, J. Seo, and S. Shin, "Probius: Automated approach for VNF and service chain analysis in software-defined NFV," in *Proceedings of the Symposium on SDN Research*, 2018, pp. 1–13.

[6] F. Schmidt, A. Gulenko, M. Wallschläger, A. Acker, V. Hennig, F. Liu, and O. Kao, "Iftm-unsupervised anomaly detection for virtualized network function services," in *2018 IEEE International Conference on Web Services (ICWS)*. IEEE, 2018, pp. 187–194.

[7] A. Elmajed, A. Aghasaryan, and E. Fabre, "Machine learning approaches to early fault detection and identification in NFV architectures," in *2020 6th IEEE Conference on Network Softwarization (NetSoft)*. IEEE, 2020, pp. 200–208.

[8] S. Zehra, U. Faseeha, H. J. Syed, F. Samad, A. O. Ibrahim, A. W. Abulfaraj, and W. Nagmeldin, "Machine learning-based anomaly detection in nfv: A comprehensive survey," *Sensors*, vol. 23, no. 11, p. 5340, 2023.

[9] J. Li, X. Qi, J. Li, Z. Su, Y. Su, and L. Liu, "Fault diagnosis in the network function virtualization: A survey, taxonomy and future directions," *IEEE Internet of Things Journal*, 2024.

[10] J. Audibert, P. Michiardi, F. Guyard, S. Marti, and M. A. Zuluaga, "Usad: Unsupervised anomaly detection on multivariate time series," in *Proceedings of the 26th ACM SIGKDD International Conference on Knowledge Discovery & Data Mining*, 2020, pp. 3395–3404.

[11] A. Chawla, P. Jacob, S. Feghhi, D. Rughwani, S. van der Meer, and S. Fallon, "Interpretable unsupervised anomaly detection for RAN cell trace analysis," in *2020 16th International Conference on Network and Service Management (CNSM)*. IEEE, 2020, pp. 1–5.

[12] J. Fan, Q. Zhang, J. Zhu, M. Zhang, Z. Yang, and H. Cao, "Robust deep auto-encoding gaussian process regression for unsupervised anomaly detection," *Neurocomputing*, vol. 376, pp. 180–190, 2020.

[13] B. Zong, Q. Song, M. R. Min, W. Cheng, C. Lumezanu, D. Cho, and H. Chen, "Deep autoencoding gaussian mixture model for unsupervised anomaly detection," in *International conference on learning representations*, 2018.

[14] Q. Xie, M.-T. Luong, E. Hovy, and Q. V. Le, "Self-training with noisy student improves imagenet classification," in *Proceedings of the IEEE/CVF Conference on Computer Vision and Pattern Recognition*, 2020, pp. 10 687–10 698.

[15] D.-H. Lee *et al.*, "Pseudo-label: The simple and efficient semi-supervised learning method for deep neural networks," in *Workshop on challenges in representation learning, ICML*, vol. 3, no. 2, 2013, p. 896.

[16] G. Pang, C. Shen, and A. van den Hengel, "Deep anomaly detection with deviation networks," in *Proceedings of the 25th ACM SIGKDD international conference on knowledge discovery & data mining*, 2019, pp. 353–362.

[17] T. DeVries and G. W. Taylor, "Dataset augmentation in feature space," *arXiv preprint arXiv:1702.05538*, 2017.

[18] Q. Du, Y. He, T. Xie, K. Yin, and J. Qiu, "An approach of collecting performance anomaly dataset for nfv infrastructure," in *Algorithms and Architectures for Parallel Processing: 18th International Conference, ICA3PP 2018, Guangzhou, China, November 15-17, 2018, Proceedings, Part III 18*. Springer, 2018, pp. 59–71.

[19] S. S. Johari, N. Shahriar, M. Tornatore, R. Boutaba, and A. Saleh, "Anomaly detection and localization in nfv systems: an unsupervised learning approach," in *NOMS 2022-2022 IEEE/IFIP Network Operations and Management Symposium*. IEEE, 2022, pp. 1–9.

[20] K. Guo, J. Chen, P. Dong, S. Liu, and D. Gao, "Fullsight: A feasible intelligent and collaborative framework for service function chains failure detection," *IEEE Transactions on Network and Service Management*, 2022.

[21] C. Sauvanaud, K. Lazri, M. Kaâniche, and K. Kanoun, "Anomaly detection and root cause localization in virtual network functions," in *2016 IEEE 27th International Symposium on Software Reliability Engineering (ISSRE)*. IEEE, 2016, pp. 196–206.

[22] L. Girish and S. K. Rao, "Anomaly detection in cloud environment using artificial intelligence techniques," *Computing*, pp. 1–14, 2021.

[23] C. Lee, J. Hong, D. Heo, and H. Choi, "Sequential deep learning architectures for anomaly detection in virtual network function chains," in *2021 International Conference on Information and Communication Technology Convergence (ICTC)*. IEEE, 2021, pp. 1163–1168.

[24] J. Hong, S. Park, J.-H. Yoo, and J. W.-K. Hong, "Machine learning based SLA-aware VNF anomaly detection for virtual network management," in *2020 16th International Conference on Network and Service Management (CNSM)*. IEEE, 2020, pp. 1–7.

[25] J. Devlin, M.-W. Chang, K. Lee, and K. Toutanova, "Bert: Pre-training of deep bidirectional transformers for language understanding," *arXiv preprint arXiv:1810.04805*, 2018.

[26] A. Diamanti, J. M. S. Vilchez, and S. Secci, "LSTM-based radiography for anomaly detection in softwarized infrastructures," in *2020 32nd International Teletraffic Congress (ITC 32)*. IEEE, 2020, pp. 28–36.

[27] L. F. Maimó, Á. L. P. Gómez, F. J. G. Clemente, M. G. Pérez, and G. M. Pérez, "A self-adaptive deep learning-based system for anomaly detection in 5G networks," *IEEE Access*, vol. 6, pp. 7700–7712, 2018.

[28] F. Michelinakis, J. S. Pujol-Roig, S. Malacarne, M. Xie, T. Dreibholz, S. Majumdar, W. Y. Poe, G. Patounas, C. Guerrero, A. Elmokashfi *et al.*, "Ai anomaly detection for cloudified mobile core architectures," *IEEE Transactions on Network and Service Management*, 2022.

[29] L. Tang, C. Xue, Y. Zhao, and Q. Chen, "Anomaly detection of service function chain based on distributed knowledge distillation framework in cloud-edge industrial internet of things scenarios," *IEEE Internet of Things Journal*, 2023.

[30] A. Chawla, A.-M. Bosneag, and A. Dalgkitsis, "Graph-based interpretable anomaly detection framework for network slice management in beyond 5g networks," in *NOMS 2023-2023 IEEE/IFIP Network Operations and Management Symposium*. IEEE, 2023, pp. 1–6.

[31] Z. Li, Y. Zhao, Y. Geng, Z. Zhao, H. Wang, W. Chen, H. Jiang, A. Vaidya, L. Su, and D. Pei, "Situation-aware multivariate time series anomaly detection through active learning and contrast vae-based models in large distributed systems," *IEEE Journal on Selected Areas in Communications*, vol. 40, no. 9, pp. 2746–2765, 2022.

[32] A. Castellani, S. Schmitt, and S. Squartini, "Real-world anomaly detection by using digital twin systems and weakly supervised learning," *IEEE Transactions on Industrial Informatics*, vol. 17, no. 7, pp. 4733–4742, 2020.

[33] J. Lu, J. Wang, X. Wei, K. Wu, and G. Liu, "Deep anomaly detection based on variational deviation network," *Future Internet*, vol. 14, no. 3, p. 80, 2022.

[34] L. Ruff, R. A. Vandermeulen, N. Görnitz, A. Binder, E. Müller, K.-R. Müller, and M. Kloft, "Deep semi-supervised anomaly detection," *arXiv preprint arXiv:1906.02694*, 2019.

[35] G. Pang, C. Shen, H. Jin, and A. v. d. Hengel, "Deep weakly-supervised anomaly detection," *arXiv preprint arXiv:1910.13601*, 2019.

[36] J. M. Sánchez, I. G. B. Yahia, and N. Crespi, "Self-modeling based diagnosis of services over programmable networks," in *2016 IEEE NetSoft Conference and Workshops (NetSoft)*. IEEE, 2016, pp. 277–285.

[37] Q. Zhu, T. Tung, and Q. Xie, "Automatic fault diagnosis in cloud infrastructure," in *2013 IEEE 5th International Conference on Cloud Computing Technology and Science*, vol. 1. IEEE, 2013, pp. 467–474.

[38] P. Bahl, R. Chandra, A. Greenberg, S. Kandula, D. A. Maltz, and M. Zhang, "Towards highly reliable enterprise network services via inference of multi-level dependencies," *ACM SIGCOMM Computer Communication Review*, vol. 37, no. 4, pp. 13–24, 2007.

[39] A. Samir and C. Pahl, “Detecting and localizing anomalies in container clusters using Markov models,” *Electronics*, vol. 9, no. 1, p. 64, 2020.
[40] Y. Zhang, Z. Guan, H. Qian, L. Xu, H. Liu, Q. Wen, L. Sun, J. Jiang, L. Fan, and M. Ke, “Cloudrca: a root cause analysis framework for cloud computing platforms,” in *Proceedings of the 30th ACM International Conference on Information & Knowledge Management*, 2021, pp. 4373–4382.
[41] C. Zhang, Z. Zhou, Y. Zhang, L. Yang, K. He, Q. Wen, and L. Sun, “Netrca: an effective network fault cause localization algorithm,” in *ICASSP 2022-2022 IEEE International Conference on Acoustics, Speech and Signal Processing (ICASSP)*. IEEE, 2022, pp. 9316–9320.
[42] C.-C. Yen, W. Sun, H. Purmehdi, W. Park, K. R. Deshmukh, N. Thakrar, O. Nassef, and A. Jacobs, “Graph neural network based root cause analysis using multivariate time-series kpis for wireless networks,” in *NOMS 2022-2022 IEEE/IFIP Network Operations and Management Symposium*. IEEE, 2022, pp. 1–7.
[43] C. Pham, L. Wang, B. C. Tak, S. Baset, C. Tang, Z. Kalbarczyk, and R. K. Iyer, “Failure diagnosis for distributed systems using targeted fault injection,” *IEEE Transactions on Parallel and Distributed Systems*, vol. 28, no. 2, pp. 503–516, 2016.
[44] K. Guo, J. Chen, P. Dong, T. Zou, J. Zhu, X. Huang, S. Liu, and C. Liao, “Dtfl: A digital twin-assisted graph neural network approach for service function chains failure localization,” *IEEE Transactions on Cloud Computing*, 2023.
[45] C. Zhang, D. Song, Y. Chen, X. Feng, C. Lumezanu, W. Cheng, J. Ni, B. Zong, H. Chen, and N. V. Chawla, “A deep neural network for unsupervised anomaly detection and diagnosis in multivariate time series data,” in *Proceedings of the AAAI Conference on Artificial Intelligence*, vol. 33, no. 01, 2019, pp. 1409–1416.
[46] D. Bahdanau, K. Cho, and Y. Bengio, “Neural machine translation by jointly learning to align and translate,” *arXiv preprint arXiv:1409.0473*, 2014.
[47] A. Terra, R. Inam, S. Baskaran, P. Batista, I. Burdick, and E. Fersman, “Explainability methods for identifying root-cause of SLA violation prediction in 5g network,” in *GLOBECOM 2020-2020 IEEE Global Communications Conference*. IEEE, 2020, pp. 1–7.
[48] S. M. Lundberg and S.-I. Lee, “A unified approach to interpreting model predictions,” in *Proceedings of the 31st international conference on neural information processing systems*, 2017, pp. 4768–4777.
[49] ”itu-ai-ml-in-5g-challenge”. [Online]. Available: https://www.ieice.org/~rising/AI-5G/
[50] [Online]. Available: https://github.com/ITU-AI-ML-in-5G-Challenge/ITU-ML5G-PS-032-KDDI-naist-lsm
[51] ”iptables”. [Online]. Available: http://ipset.netfilter.org/iptables.man.html
[52] ”suricata - open source ids/ips/nsm engine”. [Online]. Available: https://suricata-ids.org/
[53] L. Deri, M. Martinelli, T. Bujlow, and A. Cardigliano, “ndpi: Open-source high-speed deep packet inspection,” in *2014 International Wireless Communications and Mobile Computing Conference (IWCMC)*. IEEE, 2014, pp. 617–622.
[54] ”ntopng - high-speed web-based traffic analysis and flow collection”. [Online]. Available: https://www.ntop.org/products/traffic-analysis/ntop/
[55] J.-M. Kang, H. Bannazadeh, and A. Leon-Garcia, “Savi testbed: Control and management of converged virtual ict resources,” in *2013 IFIP/IEEE International Symposium on Integrated Network Management (IM 2013)*. IEEE, 2013, pp. 664–667.
[56] [Online]. Available: https://manpages.ubuntu.com/manpages/artful/man1/stress-ng.1.html
[57] [Online]. Available: https://wiki.debian.org/TrafficControl
[58] B. Settles, “Active learning literature survey,” 2009.
[59] L. Ruff, R. Vandermeulen, N. Goernitz, L. Deecke, S. A. Siddiqui, A. Binder, E. Müller, and M. Kloft, “Deep one-class classification,” in *International conference on machine learning*. PMLR, 2018, pp. 4393–4402.

Seyed Soheil Johari is a graduate researcher at the David R. Cheriton School of Computer Science, University of Waterloo. He received his B.Sc. in electrical engineering from Sharif University of Technology in 2020. He was a recipient of the best student paper award at IEEE/IFIP NOMS 2022. His research focuses on the application of machine learning techniques for data-driven management and orchestration of 5G network slices.

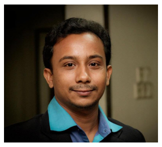

Nashid Shahriar is an assistant professor in the Department of Computer Science at the University of Regina. He received his PhD from the School of Computer Science, University of Waterloo in 2020. He was a recipient of 2020 PhD Alumni Gold Medal, 2021 Mathematics Doctoral prize, Ontario Graduate Scholarship, President’s Graduate Scholarship, and David R. Cheriton Graduate Scholarship with the University of Waterloo. His research received several recognitions, including the IEEE/IFIP NOMS 2022 Best Student Paper Award, IFIP/IEEE IM 2021 Best PhD Dissertation Award, the IEEE/ACM/IFIP CNSM 2019 Best Paper Award, IEEE NetSoft 2019 Best Student Paper Award, and the IEEE/ACM/IFIP CNSM 2017 Best Paper Award. His research interests include network virtualization, 5G network slicing, and network reliability.

Massimo Tornatore is an Associate Professor at Politecnico di Milano, Italy. He also held an appointment as Adjunct Professor at University of California, Davis, USA and as visiting professor at University of Waterloo, Canada. His research interests include performance evaluation and design of communication networks (with an emphasis on optical networking), and machine learning application for network management. He co-authored more than 400 conference and journal papers (with 19 best-paper awards) and of the recent Springer “Handbook of Optical Networks”. He is member of the Editorial Board of IEEE Communication Surveys and Tutorials, IEEE Communication Letters, IEEE Transactions on Network and Service Management and IEEE/ACM Transactions on Networking.

Raouf Boutaba (Fellow, IEEE) M.Sc. and Ph.D. degrees in computer science from Sorbonne University in 1990 and 1994, respectively. He is currently a University Chair Professor and the Director of the David R. Cheriton School of Computer science at the University of Waterloo (Canada). He also holds an INRIA International Chair in France. He is the founding Editor-in-Chief of the IEEE Transactions on Network and Service Management (2007- 2010). He is a fellow of the IEEE, the Engineering Institute of Canada, the Canadian Academy of Engineering, and the Royal Society of Canada. His research interests include resource and service management in networks and distributed systems.

Aladdin Saleh received the Ph.D. degree in electrical and electronic engineering and the M.B.A. degree in international management from the University of London, U.K. He is currently an Adjunct Professor with the Cheriton School of Computer Science, University of Waterloo. He is currently priming research and innovation activities with Rogers Communications, among them the joint research partnership with the University of Waterloo on 5G and emerging technologies. He has over 20 years of industry experience in mobile telecom in Canada. He taught and conducted research on next-generation wireless networks at several universities as a full-time Professor, an Adjunct Professor, and a Visiting Researcher.